Journal of Power Sources 196 (2011) 8307–8312

Contents lists available at ScienceDirect

Journal of Power Sources

journal homepage: www.elsevier.com/locate/jpowsour

Particle shape control using pulse electrodeposition: Methanol oxidation as a probe reaction on Pt dendrites and cubes

Irene J. Hsu, Daniel V. Esposito, Elizabeth G. Mahoney, Andrew Black, Jingguang G. Chen*

Department of Chemical Engineering, Center for Catalytic Science and Technology, University of Delaware, Newark, DE 19716, United States

ARTICLE INFO

Article history:
Received 22 April 2011
Received in revised form 9 June 2011
Accepted 10 June 2011
Available online 17 June 2011

Keywords:
Platinum
Tungsten carbide
Electrodeposition
Methanol oxidation
Shape control synthesis

ABSTRACT

Shape controlled Pt particles were synthesized onto tungsten monocarbide (WC) substrates using a pulse electrodeposition method. The particle shape was strongly influenced by the deposition potential, with cubic particles formed using 0.14 V vs. NHE (normal hydrogen electrode) and dendritic particles formed at 0.04 V vs. NHE. The crystalline orientation and active surface area of the Pt particles were estimated using Cu stripping voltammetry. Finally, cyclic voltammetry and chronoamperometry were used to determine the methanol electrooxidation activity, which revealed that the dendritic Pt showed much higher electrochemical activity than the cubic particles. These results demonstrated the possibility of more effectively utilizing Pt electrocatalysts by controlling the shape of Pt particles.

1. Introduction

In catalyst synthesis, the structure of the particle is often overlooked. Rather, the focus is often on producing catalysts that are the smallest size to improve the ratio of exposed surface area per precious metal loading while keeping precious metal loadings as low as possible. For some reactions that have been shown to be structure sensitive, another way to optimize the catalyst is to synthesize metal particles with specific shapes. For example, Pt nanoparticles have been shown to effectively oxidize methanol, but their morphology and surface crystalline orientation have been found to play a considerable role in their effectiveness [1]. The methanol oxidation reaction is a structure sensitive reaction, and certain crystal planes have been shown to exhibit higher activity than others [2,3]. Therefore, a method to produce Pt particles with shape control can be useful in optimizing the methanol oxidation reaction activity.

Colloidal methods using organic ligand stabilizers are one of the most commonly used methods in making shape controlled particles [4–8]. However, the organic ligand shells can be difficult to remove and can inhibit catalytic activity [9]. In contrast, electrochemical deposition is a fast, simple method that can produce three-dimensional particles directly onto a substrate or support. It is a one-step technique, requires no additional purification step, and its implementation is low in cost with commercially available technology [10–12]. It also has the added benefit of being applicable on a number of support geometries, as the deposition process is not a line-of-sight method. Furthermore, the deposition potential has been shown to be a convenient parameter for controlling the structure of the deposited metal [13]. Electrodeposition has been used to demonstrate the production of metallic particles of various shapes on a number of substrates. For example, the electrodeposition of chromium particles was demonstrated on Si, making spherical particles at low deposition potentials and hexagonal microrods at higher potentials [14]. Another example is the synthesis of tetrahexahedral Pd nanocrystals with high Miller index facets using a pulse electrodeposition method [15].

For most electrocatalytic application the chosen support can have a large influence on the effective use of the catalyst. This is especially true for supporting electrodeposited catalyst particles, since the nature of the catalyst can strongly affect particle nucleation [16]. In this work, we explore the use of tungsten monocarbide (WC) as a supporting material. Because of its similar bulk electronic properties to Pt, WC has been identified as a promising substrate to support Pt catalysts, exhibiting improved performance compared to carbon substrates [17–21]. It is inexpensive, electrically conductive, and durable in acidic environments [20,21]. WC has previously been demonstrated to be a good support for Pt for several types of electrochemical reactions. For example, one monolayer of Pt on a WC substrate was found to have comparable activity for the hydrogen evolution reaction as bulk Pt [19]. The monolayer bimetallic system maximizes the use of the Pt catalyst by replacing the bulk of the catalyst with WC, leaving one monolayer of Pt to act as the catalyst for the reaction. Furthermore, it has been observed that

* Corresponding author. Tel.: +1 302 831 0642; fax: +1 302 831 1048.
E-mail address: jgchen@udel.edu (J.G. Chen).

0378-7753/$ – see front matter © 2011 Elsevier B.V. All rights reserved.
doi:10.1016/j.jpowsour.2011.06.043

Pt on a WC support maintains more of its electrochemically active surface area after rigorous potential cycling than Pt supported on carbon [17]. This suggests that Pt on a WC support is more resistant to catalyst degradation issues commonly seen on commercial Pt/C catalysts such as particle agglomeration and dissolution [17].

The aim of this work is to demonstrate the ease of pulse electrodeposition as a method to produce a variety of particles shapes and confirm the effect that this can have on the activity of methanol oxidation, a structure sensitive reaction. Here, pulse electrodeposition is utilized to synthesize Pt particles that are round, cubic, or dendritic, depending on the deposition potential. The preferred crystal orientations of the particles are confirmed with Cu stripping voltammetry and correlated with methanol oxidation activity to demonstrate the effects of Pt crystal planes on the electrooxidation activity.

2. Experimental

WC thin films were produced on W foils using a carburization technique previously detailed elsewhere [22]. Pt electrodeposition was carried out using a three-electrode cell and a Princeton Applied Research Potentiostat/Galvanostat Model 263A at room temperature (~25 °C). A saturated calomel electrode (SCE) was used as the reference and Pt gauze as the counter electrode. All results are presented with respect to the normal hydrogen electrode (NHE). All solutions were prepared using deionized water purified with a Barnstead NANO pure filtration system to a conductivity of ~18 MΩ cm^{-1}. The electrolyte, a 2 mM $H_2PtCl_6{\cdot}6H_2O$ (Aldrich) and 0.1 M H_2SO_4 (Fischer Scientific) solution, was first deaerated with high purity N_2 for 20 min. Nitrogen was swept through the headspace to prevent oxygen or any other impurities from entering the cell during deposition.

SEM images were obtained using a 7400f JEOL field emission gun scanning electron microscope with an accelerating voltage of 3 kV. Electrochemical characterization was carried out at room temperature in the same three-electrode cell set up as deposition. Before measurements, electrodeposited Pt–WC samples were prepared by dipping into 0.3 M NaOH solution to remove any tungsten oxides [22], followed by a rinse with acetone, methanol, and deionized water and dried with high purity nitrogen. All electrolyte solutions were deaerated with high purity nitrogen prior to measurements, with a nitrogen sweep during experiments. Upon submerging in electrolyte solution, the working electrode samples were cycled from 0 V to 0.8 V vs. NHE at 10 mV s^{-1} for 10 cycles to clean the electrode surface before electrochemical measurements. Methanol electooxidation tests were performed in a solution of 0.1 M H_2SO_4 and 0.2 M CH_3OH (Fischer Scientific). Chronoamperometry (CA) measurements were conducted at a potential of 0.84 V vs. NHE over 200 s. Cyclic voltammograms were collected using a scan rate of 50 mV s^{-1}. Copper stripping voltammetry was done using an electrolyte solution of 2 mM $CuSO_4$ (Fischer Scientific) and 0.1 M H_2SO_4. The working electrode was held at a potential of 0.32 V for 2 min to allow the Cu atoms to adsorb onto the Pt surfaces. The adsorbed Cu was then stripped by scanning from 0.32 V to 0.9 V. All linear scans were measured using a scan rate of 100 mV s^{-1}. A background scan was also measured in 0.1 M H_2SO_4 from 0.3 V to 0.9 V using a scan rate of 100 mV s^{-1}. The background scan was subtracted from the Cu stripping scan to produce a difference curve, which was then integrated to obtain the Cu stripping charge.

3. Results and discussion

3.1. Electrodeposition and characterization

In pulse electrodeposition the electrode potential is alternated between periods of high overpotential, which promotes nucleation, and low overpotential, which allows the existing nuclei to grow [23]. Compared to an electrodeposition performed at a single potential, the pulse deposition method can provide more uniform particles that are more evenly dispersed on the substrate [16]. During the constant potential electrodeposition process, the nucleation and growth processes compete with one another, causing particle dispersion to increase with increasing deposition time. Both the nucleation and growth processes are influenced by the surface diffusion rates of the plating ions as well as the rate of charge transfer between the substrate and ions in solution. When there are low surface diffusion rates and fast charge transfer, nucleation is favored; conversely, when the surface diffusion rate is high and the charge transfer rate is slow, there is particle growth [23]. In comparison, pulse electrodeposition allows the user to alternate between these two regimes, providing a balance between nucleation and particle growth. For the pulse depositions in this work, a number of 30 pulse iterations were specified, with one iteration comprised of the following sequence: 5 s at the high overpotential followed by 5 s at the low overpotential. The overpotential is defined as the difference between the electrode potential and the reversible potential for the Pt(IV)/Pt(0) coupling (E_{Pt}~0.7 V vs. NHE) [13]. Table 1 lists the potentials used for each experiment, as well as the resulting particle shape.

Fig. 1 shows SEM images of the particles that were produced using the pulse potentials listed in Table 1. Insets show a higher magnification image that more clearly reveals the shapes of the Pt particles. The first three samples were synthesized using a low overpotential (E_2) of 0.64 V, close to E_{Pt}, so the particles should have similar growth rates. The high overpotential pulse (E_1) is in the range between 0.24 V and 0.04 V, corresponding to ~0.5–0.7 V overpotential. When the lowest deposition overpotential (E_1 = 0.24 V) is used, as with Sample 1a (Fig. 1a), rounded particles are produced. At a slightly larger overpotential, E_1 = 0.14 V, enough current transfer is provided for Pt to nucleate into cubic structures such as Sample 1b (Fig. 1b). At an even larger overpotential (E_1 = 0.04 V), the faster nucleation rate results in the formation of particles with short dendrites (Fig. 1c). These are similar to what has been referred to as flowers in other Pt deposition studies, which used a static potential electrodeposition method [10–12]. Sample 1d, uses the same high deposition overpotential as Sample 1c (E_1 = 0.04 V) but with a less positive potential during the growth pulse (E_2 = 0.56 V). Because of the larger overpotential during the growth pulse, the increased growth rate makes the mass-transfer of Pt ions more limiting, which is favorable for dendritic growth [24]. The incoming Pt ions deposit on the first available surface, which is typically farthest from the WC substrate on the edge of an existing Pt particle. This promotes outward growth, creating long dendrites. Compared with Sample 1c that has a slow growth rate, this more spontaneous growth period allows the dendrites to grow longer, resulting in the more pronounced spiked features seen in Fig. 1d.

TEM images (Fig. 2) allow closer inspection of the particles as well as determination of some of the Pt crystal planes that are present. Fig. 2a shows a dendritic particle, while Fig. 2b is a high resolution image of the end of one of the dendrites in Fig. 2a indicated by the boxed area. Lattice fringes can be seen in the Fig. 2b and are measured to be close to 2.27 Å, corresponding to the d-spacing for Pt(1 1 1). Additionally, a fast Fourier transform of the high resolution image shows a simulated diffraction pattern that represents a [1 1 1]-type direction, further demonstrating that the dendrites are generally (1 1 1)-oriented. Fig. 2c and d shows TEM images of the cubic particles, and the insert shows a selected area electron diffraction pattern of the sample in Fig. 2c. This diffraction pattern shows a [1 0 0]-type pattern, consistent with what is expected for a cube structure.

Table 1
List of pulse potential experiments using 2 mM H_2PtCl_6/0.1 M H_2SO_4. Sample number corresponds to Fig. 1.

Sample	High overpotential pulse, E_1 (V vs. NHE)	Low overpotential pulse, E_2 (V vs. NHE)	General particle shape	Electrochemically active surface area (cm^2)
1a	0.24	0.64	Round	0.98
1b	0.14	0.64	Cube	1.65
1c	0.04	0.64	Short dendrites	6.65
1d	0.04	0.54	Long dendrites	12.40

3.2. Determination of surface area using Cu stripping

One interesting characteristic of the dendritic particles is that their extension into space increases the active surface area of the catalyst, and can therefore maximize the overall methanol oxidation activity [11]. To determine the surface area of the various Pt particle shapes, Cu stripping voltammetry was utilized because it is effective in determining the Pt surface area without taking the WC substrate into consideration. Other methods that can determine the electrochemically active surface area, such as CO stripping voltammetry and the underpotential deposition (UPD) of hydrogen, have overlapping features representing both Pt and WC, making it difficult to differentiate which features correspond to Pt or WC. During Cu stripping voltammetry, the UDP of Cu takes place on the surface of the Pt particles. The resulting Cu monolayer is then stripped away, and the resulting charge can then be divided by 420 $\mu C\,cm^{-2}$, the generally accepted value for 2-electron charge transfer on polycrystalline Pt [25], to determine the electrochemically active surface [26].

For UPD of a metal to take place on a given substrate, the metal–substrate interaction must be favored over the metal–metal interaction. Otherwise, bulk deposition will occur. The Cu–Pt interaction is strong enough for Cu UPD to take place on Pt; conversely, the Cu–WC is too weak for such a deposition to transpire [27]. There is no discernable difference between the Cu stripping curve on WC compared to the background scan. Using this method, the electrochemically active surface area of each Pt particle shape was determined. These values are summarized in Table 1 and shows that the dendritic particles have much higher electrochemically active surface areas than the round and cubic particles. Furthermore, the surface area of the particles with long dendrites (1d) are nearly twice that of the particles with short dendrites (1c), showing the advantage of longer dendritic particles in maximizing active surface area compared to the other particle shapes.

Because SEM and TEM images show only a small percentage of the entire sample, it is necessary to confirm the preferred orientation of the sample with a method that can sample all of the deposited particles. In addition to determining the electrochemically active surface area of Pt, Cu stripping voltammograms can also be used to determine the preferred crystal orientation of each deposition sample. The peak positions of the Cu stripping curves (Fig. 3) are characteristic of crystal planes that are present in the sample, similar to how the hydrogen adsorption peaks in a Pt cyclic voltammogram in an acidic solution each represent different crystal planes that are present [26,28–31]. The area of each peak is also an indication of the quantity of each crystal plane, and the preferred orientation can be determined by comparing the peak areas [28–31]. The peaks in the Cu stripping measurements in Fig. 3 are broad because these samples contain a number of defects, steps, and other imperfections. Furthermore, the formation of UPD Cu is a complicated mechanism involving surface reconstructions at the (1 1 0) and (1 0 0) crystal planes which can bring about peaks at different locations stemming from Cu atoms moving to different surface configurations [32]. Regardless, each particle shape has its

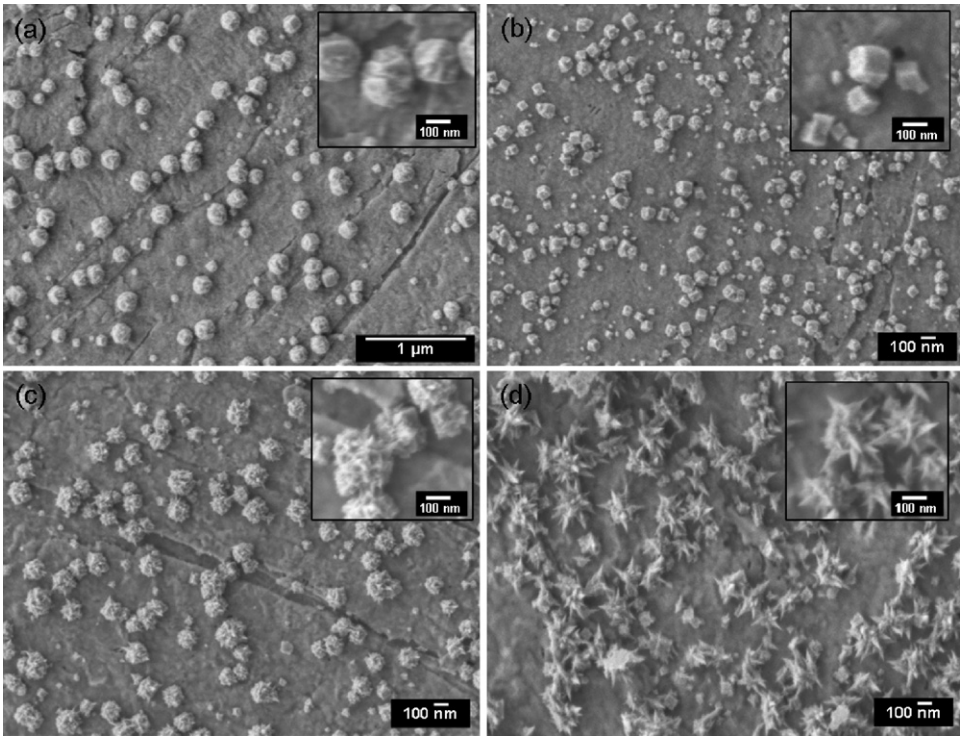

Fig. 1. SEM images of Pt particle electrodeposited using a range of potentials corresponding to Table 1: (a) 1a, (b) 1b, (c) 1c, and (d) 1d.

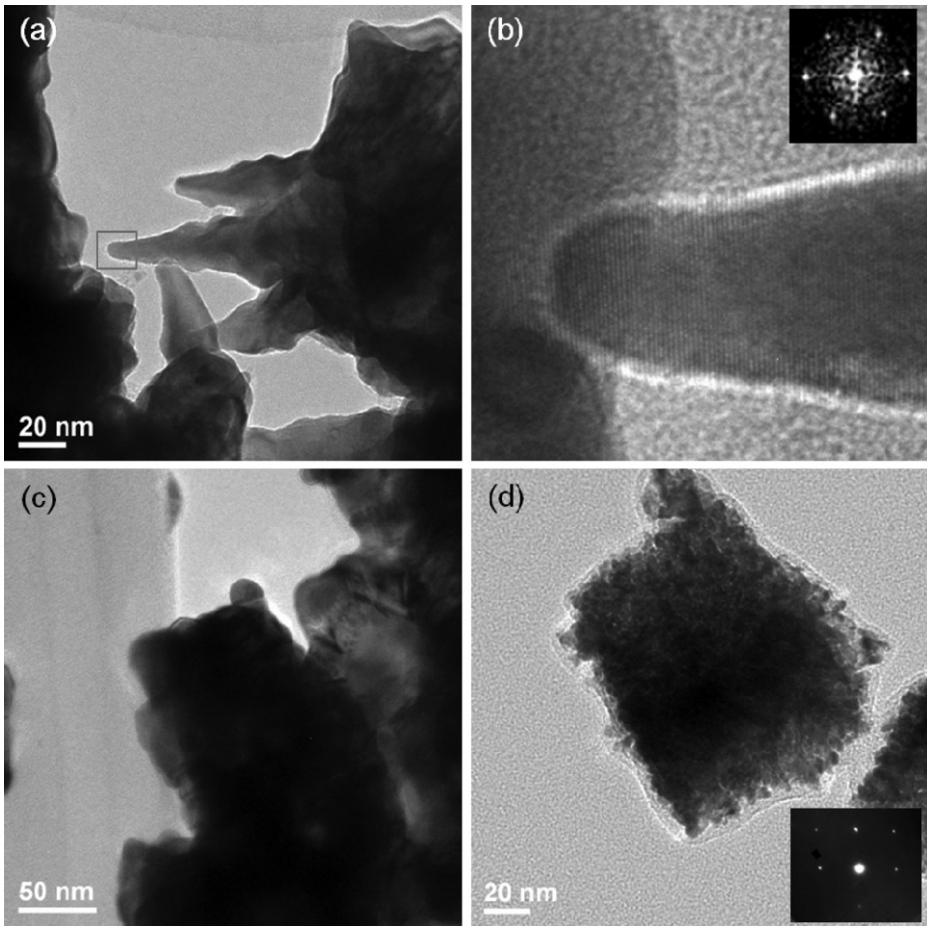

Fig. 2. (a) TEM image of a dendritic particle, and (b) high resolution image of the end of one of the dendrites in (a). The inset shows a fast Fourier transform of image. (c) and (d) TEM images of the cubic particles. The inset in (d) shows a selected area electron diffraction pattern of the sample.

own distinct Cu stripping voltammogram that gives a good indication of its preferred crystal orientation. There are three main peaks among the Cu stripping voltammograms shown in Fig. 3. Comparing to previous Cu underpotential deposition studies on Pt single crystals, the first broad peak at 0.42 V represents the (1 0 0) crystal plane, while the peak at around 0.55 V corresponds to the (1 1 0) plane and the last peak at 0.67 V signifies the (1 1 1) direction [32–35]. The round particles (Fig. 3a) have a broad feature that covers the whole region, indicating that all three crystal orientations are present and that there is no preferred orientation. The cubic particles (Fig. 3b) show peaks in the 0.4–0.55 V potential region, mostly around 0.42 V. This indicates that the cubic particles are predominantly (1 0 0) terminated, which is expected for an fcc unit cell such as that for Pt. This is also confirmed with the TEM image in Fig. 2c and d. The Cu stripping curve for the dendritic particles (Fig. 3c and d) contain all three peaks. However, the long dendrite sample (Fig. 3d) has one peak that is the most pronounced at 0.67 V, suggesting that the particles are largely oriented in the (1 1 1) direction. These particles are dominated by the dendritic spikes growing in the most energetically favorable direction, which for an fcc unit cell is the (1 1 1) direction, and this too confirms the TEM data (Fig. 2a and b). Overall, the Cu stripping voltammograms in Fig. 3 indicate that the cubic particles are mostly (1 0 0) oriented, while the dendrites are preferentially (1 1 1) oriented.

3.3. Methanol oxidation as a structure sensitive probe reaction

Methanol oxidation, previously shown to be a structure sensitive reaction [2,3], was used as a probe reaction to demonstrate the activity of the Pt particles with varying shapes. Cyclic voltammograms (CV) of the dendritic and cubic particles in 0.2 M CH_3OH/0.1 M H_2SO_4 is shown in Fig. 4a. All cyclic voltammograms are normalized with respect to the Pt surface area, so the current densities can be compared as a qualitative measure of activity. Methanol oxidation is typically denoted by a peak at around 0.82–0.86 V in the forward scan, and a second oxidation peak representing the removal of carbonaceous species that lead to CO poisoning is seen at around 0.72–0.76 V in the reverse scan [12,36]. The dendritic particles show much higher methanol oxidation activity than the cubic particles. Previous work with Pt nanoflowers and dendritic particles have shown that these particles have enhanced activity compared to Pt nanoparticles supported on carbon [10–12], and work using preferentially oriented particles showed that those particles containing mostly (1 1 1) planes generally have higher activities compared to those dominated by (1 0 0) planes [3,37]. This is consistent with the results in Fig. 4a. In Fig. 4a, features representing hydrogen UPD in the low potential region (between 0 V and 0.4 V) verify the presence of Pt on the cubic sample, and the width of the voltammogram in this region is comparable to the width of same region for the dendritic sample. This should be expected since these CV curves were normalized with respect to the Pt surface area. It is more likely that the methanol oxidation activity generated by the cubic Pt sample is so small that the methanol oxidation feature is overwhelmed by the large tungsten oxidation peak at higher potentials (0.8–1.0 V). The reason for the higher methanol oxidation activity on the dendritic Pt may be its ability to oxidize CO more efficiently than the cubic particles. Previous work has found that Pt nanoparticles with (1 1 1) orien-

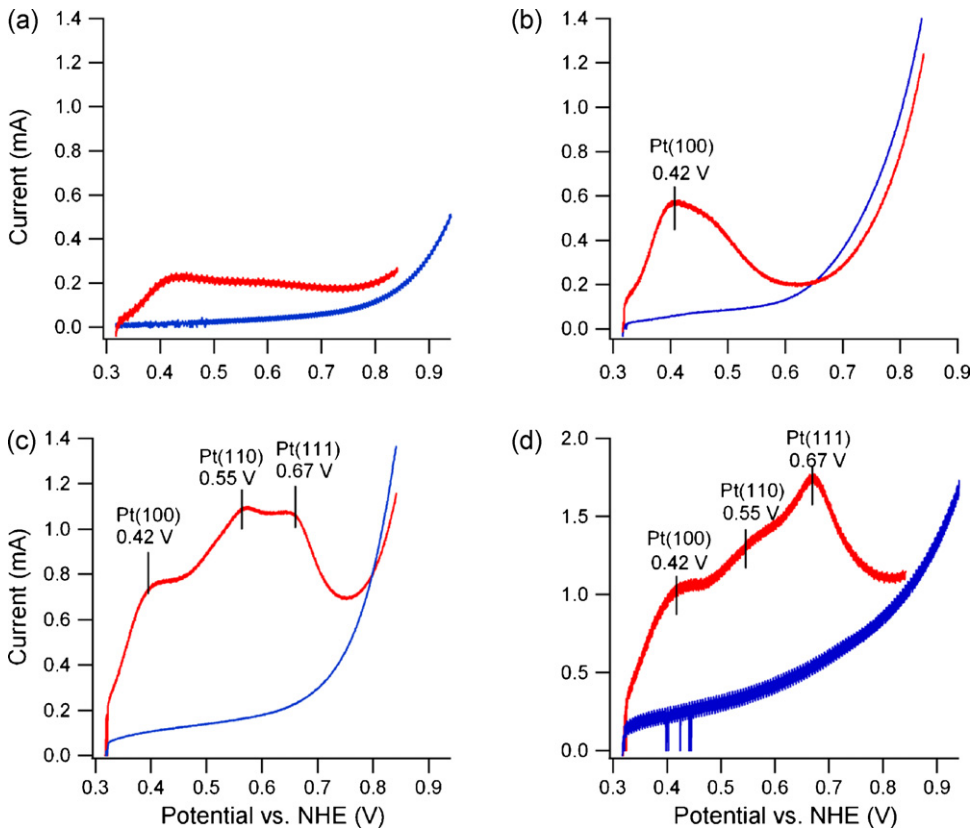

Fig. 3. Copper stripping voltammograms corresponding to (a) round, (b) cubic, (c) short dendritic, and (d) long dendritic particles. Red lines show the Cu stripping scan; blue lines are background scans. (For interpretation of the references to color in this figure legend, the reader is referred to the web version of the article.)

tation are generally more CO tolerant than Pt nanoparticles with (1 0 0) orientation, and this generally leads to higher methanol oxidation activity [3,11]. For example, a study using dendritic Pt on silicon substrates show that the onset potential and peak potential of CO stripping voltammograms using dendritic nanoflower Pt is lower than that of spherical Pt particles, indicating that the Pt dendrites oxidizes CO more efficiently than Pt nanoparticles, ultimately leading to enhanced methanol oxidation activity because more sites are available for reaction [11].

In CV measurements, the capacitive currents contribute to the intensity of the anodic oxidation peaks [38], making it difficult to quantitatively compare the activities from CV curves. In order to determine the steady state methanol oxidation activity chronoamperometry (CA) measurements were performed at a potential of 0.84 V (close to the methanol oxidation peaks), as shown in Fig. 4b. The normalized current densities at the end of the 200-s experiment are 139 and 64 $\mu A\,cm^{-2}$ for dendritic and cubic particles, respectively. These results are in agreement with the CV results in Fig. 4a that dendritic particles have considerably higher methanol oxidation activity than cubic particles. This is also in agreement with literature exploring nanoparticles of varying (1 1 1) and (1 0 0) ratios, which show the same trend [3].

For the methanol oxidation reaction, the dendritic (1 1 1)-oriented Pt catalysts are preferred over cubic (1 0 0)-oriented Pt because they exhibit enhanced activity. However, cubic Pt particles will be desired for reactions that are more easily catalyzed by Pt(1 0 0) surfaces. For example, Pt nanocubes made using colloidal methods have been shown to produce enhanced oxygen reduction activity over other Pt nanoparticle shapes [8], and the electrodeposited cubic Pt is expected to outperform the dendritic

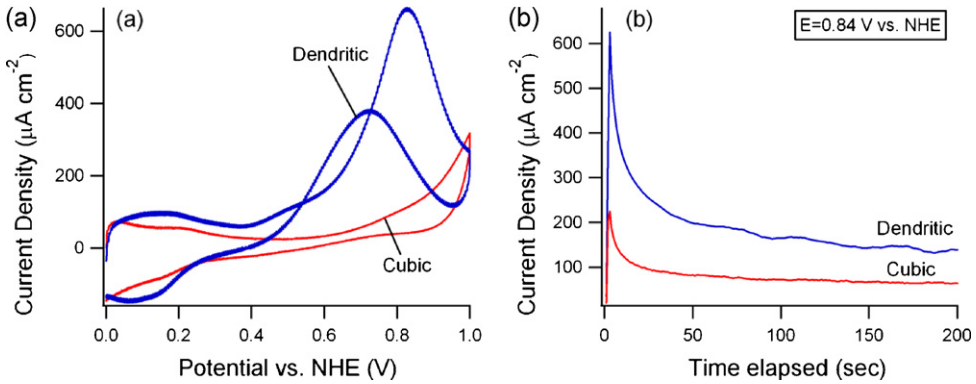

Fig. 4. (a) Cyclic voltammograms of dendritic and cubic Pt particles on WC. Voltammograms were done in 0.2 M CH_3OH and 0.1 M H_2SO_4, and the scan rate was 50 mV s^{-1}. The 50th cycles are presented. (b) Chronoamperometry measurements of dendritic and cubic particles in 0.2 M CH_3OH and 0.1 M H_2SO_4.

particles for this reaction. Results in the current study demonstrate the feasibility of producing particles with predominantly (1 0 0) or (1 1 1) orientations using a simple and controlled method. To the best of our knowledge, no other method besides the one described here has been reported to easily and successfully produce both (1 1 1)-oriented and (1 0 0)-oriented Pt catalysts without the use of additives or organic stabilizers. In addition, the deposition of Pt on the WC substrates has the potential advantages of using a cheap and stable substrate that has been shown to have success as supports for Pt for fuel cell applications.

4. Conclusions

A variety of Pt particle shapes were produced on WC substrates using a pulse electrodeposition technique with the deposition potential being the main control parameter. The control over the particle shape is advantageous because it should allow the catalyst to be used more efficiently for a variety of structure sensitive reactions. To make cubic particles, a deposition potential of 0.14 V was needed to balance nucleation and growth in the (1 0 0) direction. Dendritic particles were made when the nucleation pulse overpotential was high (0.04 V), and dendrites were allowed to grow longer during a higher overpotential growth period. Cu stripping voltammetry confirms that these particles show a preferred orientation–cubic particles are mostly (1 0 0) oriented, while dendrites are mostly (1 1 1). Finally, enhanced methanol oxidation activity was observed with the (1 1 1) dendritic particles using CV and CA over the cubic particles, which showed very little methanol oxidation activity. While the Pt particles produced here are considerably larger than what is typical for a fuel cell catalyst, they are used in the current study to demonstrate the shape control aspect of the pulse electrodeposition method and it is easier to see the exact shapes with larger particles. Since the methanol oxidation experiments were performed using these large particles, the mass specific activity will be smaller than what is typically observed for nanoparticle catalysts. However, the combined synthesis and characterization results provide useful input in more efficiently utilizing Pt electrocatalysts by controlling the shapes of Pt particles.

References

[1] A. Santasalo, F.J. Vidal-Iglesias, J. Solla-Gullón, A. Berná, T. Kallio, J.M. Feliu, Electrochim. Acta 54 (2009) 6576–6583.
[2] N.M. Markovic, P.N. Ross, Surf. Sci. Rep. 45 (2002) 117–229.
[3] J. Solla-Gullon, F.J. Vidal-Iglesias, A. Lopez-Cudero, E. Garnier, J.M. Feliu, A. Aldaz, Phys. Chem. Chem. Phys. 10 (2008) 3689–3698.
[4] T.S. Ahmadi, Z.L. Wang, T.C. Green, A. Henglein, M.A. El-Sayed, Science 272 (1996) 1924–1927.
[5] R. Narayanan, M.A. El-Sayed, J. Am. Chem. Soc. 126 (2004) 7194–7195.
[6] J. Ren, R.D. Tilley, J. Am. Chem. Soc. 129 (2007) 3287–3291.
[7] M. Tsuji, P. Jiang, S. Hikino, S. Lim, R. Yano, S.-M. Jang, S.-H. Yoon, N. Ishigami, X. Tang, K.S.N. Kamarudin, Colloids Surf. A 317 (2008) 23–31.
[8] C. Wang, H. Daimon, Y. Lee, J. Kim, S. Sun, J. Am. Chem. Soc. 129 (2007) 6974–6975.
[9] B. Zhang, C. Zhang, H. He, Y. Yu, L. Wang, J. Zhang, Chem. Mater. 22 (2010) 4056–4061.
[10] H.M. Zhang, W.Q. Zhou, Y.K. Du, P. Yang, C.Y. Wang, Electrochem. Commun. 12 (2010) 882–885.
[11] J.N. Tiwari, R.N. Tiwari, K.-L. Lin, ACS Appl. Mater. Interfaces 2 (2010) 2231–2237.
[12] L. Tian, Y. Qi, B. Wang, J. Colloids Interface Sci. 333 (2009) 249–253.
[13] L.M. Plyasova, I.Y. Molina, A.N. Gavrilov, S.V. Cherepanova, O.V. Cherstiouk, N.A. Rudina, E.R. Savinova, G.A. Tsirlina, Electrochim. Acta 51 (2006) 4477–4488.
[14] L.Y. Zhao, A.C. Siu, L.J. Pariag, Z.H. He, K.T. Leung, J. Phys. Chem. C 111 (2007) 14621–14624.
[15] N. Tian, Z.Y. Zhou, N.F. Yu, L.Y. Wang, S.G. Sun, J. Am. Chem. Soc. 132 (2010) 7580–7581.
[16] T. Brülle, U. Stimming, J. Electroanal. Chem. 636 (2009) 10–17.
[17] H. Chhina, S. Campbell, O. Kesler, J. Power Sources 164 (2007) 431–440.
[18] H. Chhina, S. Campbell, O. Kesler, J. Power Sources 179 (2008) 50–59.
[19] D.V. Esposito, S.T. Hunt, A.L. Stottlemyer, K.D. Dobson, B.E. McCandless, R.W. Birkmire, J.G. Chen, Angew. Chem. Int. Ed. 49 (2010) 9859–9862.
[20] H.H. Hwu, J.G. Chen, Chem. Rev. 105 (2005) 185–212.
[21] A.L. Stottlemyer, E.C. Weigert, J.G. Chen, Ind. Eng. Chem. Res. 50 (2011) 16–22.
[22] M.C. Weidman, D.V. Esposito, I.J. Hsu, J.G. Chen, J. Electrochem. Soc. 157 (2010) F179–F188.
[23] H. Kim, N.P. Subramanian, B.N. Popov, J. Power Sources 138 (2004) 14–24.
[24] K. Fukami, S. Nakanishi, H. Yamasaki, T. Tada, K. Sonoda, N. Kamikawa, N. Tsuji, H. Sakaguchi, Y. Nakato, J. Phys. Chem. C 111 (2006) 1150–1160.
[25] S. Trasatti, O.A. Petrii, Pure Appl. Chem. 63 (1991) 711–734.
[26] C.L. Green, A. Kucernak, J. Phys. Chem. B 106 (2002) 1036–1047.
[27] M.D. Obradovic, B.M. Babic, A. Kowal, V.V. Panic, S.L.J. Gojkovic, J. Serb. Chem. Soc. 73 (2008) 1197–1209.
[28] E.G. Ciapina, S.F. Santos, E.R. Gonzalez, J. Electroanal. Chem. 644 (2010) 132–143.
[29] S. Garbarino, A. Ponrouch, S. Pronovost, J. Gaudet, D. Guay, Electrochem. Commun. 11 (2009) 1924–1927.
[30] V. Grozovski, J. Solla-Gullón, V.c. Climent, E. Herrero, J.M. Feliu, J. Phys. Chem. C 114 (2010) 13802–13812.
[31] J. Solla-Gullon, P. Rodriguez, E. Herrero, A. Aldaz, J.M. Feliu, Phys. Chem. Chem. Phys. 10 (2008) 1359–1373.
[32] A. Danilov, R. Nazmutdinov, T. Zinkicheva, E. Molodkina, A. Rudnev, Y. Polukarov, J. Feliu, Russ. J. Electrochem. 44 (2008) 697–708.
[33] O. Endo, N. Ikemiya, M. Ito, Surf. Sci. 514 (2002) 234–240.
[34] R. Francke, V. Climent, H. Baltruschat, J.M. Feliu, J. Electroanal. Chem. 624 (2008) 228–240.
[35] G. Jerkiewicz, F.d.r. Perreault, Z. Radovic-Hrapovic, J. Phys. Chem. C 113 (2009) 12309–12316.
[36] R. Mancharan, J.B. Goodenough, J. Mater. Chem. 2 (1992) 875–887.
[37] Q. Shen, L. Jiang, H. Zhang, Q. Min, W. Hou, J.-J. Zhu, J. Phys. Chem. C 112 (2008) 16385–16392.
[38] E.C. Weigert, A.L. Stottlemyer, M.B. Zellner, J.G. Chen, J. Phys. Chem. C 111 (2007) 14617–14620.